Effect of Reinforcement Stiffeners on Square Concrete-filled Steel Tubular Columns Subjected to Axial Compressive Load

Yuanlong Yang [a], Yuyin Wang [b,*], Feng Fu [c]

([a] Key Laboratory of Mechanics on Disaster and Environment in Western China of China Ministry of Education, Lanzhou University, Lanzhou 730000, China;
[b] School of Civil Engineering, Harbin Institute of Technology, Harbin 150090, China;
[c] School of Engineering and Mathematical Sciences, City University, London, EC1V 0HB, U.K.)

Abstract. Eight stiffened square concrete-filled steel tubular (CFST) stub columns with slender sections of encasing steel and two non-stiffened counterparts were tested subjected to axial compressive load. Four types of reinforcement stiffeners and steel tensile strips were introduced to postpone local buckling of steel tubes, in which the tensile strip was first used as stiffener in CFSTs. The stiffening mechanism, failure modes of concrete and steel tubes, strength and ductility of stiffened square CFSTs were also studied during the experimental research. A numerical modeling program was developed and verified against the experimental data. The program incorporates the effect of the stiffeners on postponing local buckling of the tube and the tube confinement on concrete core. Extensive parametric analysis was also conducted to examine the influencing parameters on mechanical properties of stiffened square CFSTs.

Keywords: concrete-filled steel tube, axial compressive load, stiffener, local buckling, confinement

1. Introduction

In structural systems using square concrete-filled steel tubular (CFST) columns, regular indoor space is provided and joint construction is facilitated and fast tracked. However, the lateral pressure from square steel tube is unevenly distributed in the square concrete cross-section. The lateral pressure near the web centers is weaker than that near the corners. On the other hand, the steel tube is prone to buckle, especially when depth-to-thickness ratio is large. These disadvantageous

* Corresponding author: Yuyin Wang, Email: wangyuyin@hit.edu.cn; Tel./Fax: +86 451 86282083

mechanical behaviors of concrete and steel tube mentioned above can attribute to their inadequate interaction. To enhance the interaction between the steel and concrete and further increase their resistances, other scholars introduced stiffeners into square CFSTs. The patterns of stiffeners are shown in authors' previous paper [1].

The plate rib is the most commonly used stiffener in square CFST columns. Experimental studies were carried out to investigate its anti-buckling behavior [2][3][4]. The plate ribs are welded on the inner surfaces of the tube to reinforce the tube by enlarging bending rigidity of steel plate sections. After the HyogokenNanbu earthquake, the plate rib was introduced in bridge piers and frame columns with huge cross-sections [5]. To simplify fabricating procedure, stiffeners sometimes can be formed by bending steel plates. Curling ribs and oblique curling ribs were studied in the experiments [6] [7] by welding cold-formed channels or isosceles angle irons with curling edges. Test results show that, under low compression ratio, the curling ribs and oblique curling ribs can effectively improve static ultimate strength and enhance ductility of the structure in resisting earthquake load. However, the embedment of these ribs in concrete, depending on frictional force between stiffeners and concrete, cannot guarantee the interaction between the concrete and steel tube, and is also weakened by concrete expansion. Meanwhile, the full penetration butt weld may lead to residual stresses in steel plates. Curling ribs may also encounter fabricating problems in bending curling edges, especially for thick plates.

To improve the embedment of stiffeners in concrete, other types of stiffeners, mainly employing steel tensile property, were introduced into square CFST columns. Studies on performance of square CFST members, by utilizing pairs of tie rods, also known as binding bars, at possible plastic hinge locations, were conducted in [8, 9]. Constitutive relationship was developed for square CFSTs with binding bars [10], in which, the concrete constitutive relationship took a similar form to

that of Mander model. However, the convex tie rods obstruct indoor space. To improve this disadvantage, tension sheets was introduced with similar stiffened scheme [6]. Furthermore, oblique tie bars, as an enhanced stiffened scheme by decreasing welding spacing in cross section, was employed [11]. The stiffeners, such as tie rods, binding bars and oblique tie bars, can effectively avoid concrete cracking, restrain the out-of-plane deformation of plates and therefore delay local buckling of steel tubes.

The previous research showed that the proposed stiffeners can obviously delay local buckling of the tube and provide enhanced strength and ductility compared to square CFST columns. However, the existing stiffeners may have limitations in material efficiency or fabrication feasibility. Innovative types of reinforcement stiffeners were proposed in authors' previous experimental research [1] in 2012. Preliminary results on behavior of reinforcement stiffeners were obtained. It is found that, some types of reinforcement stiffeners can increase steel tensile capacity, however, the remaining types cannot.

The study in this paper was performed to investigate the static behavior of square CFST cross-sections with reinforcement stiffeners or tensile strips. On the basis of previous tests conducted by the authors, the post-buckling properties and constraint effect for concrete were studied. Both experimental and analytical researches were carried out to assess of the proposed stiffeners. Numerical analysis was made on stiffened square CFST cross-sections to study various parameters such as material strengths, material consumptions and stiffener arrangement type.

Compared to the previous research [1], material efficiency was achieved by promoting improved stiffened scheme for steel tubes in this paper. The steel tensile strip was first used as stiffener in the CFSTs. The range of steel tube ratio to the concrete was extended to get more behavioral understanding of CFST specimens. Loading devices were improved to stably record the

load-displacement curves during load descending stage. Based on the test observation, local buckling was included in the strength of steel tubes in numerical analysis.

2. Experimental program

2.1 Test specimens

Table 1 summarizes the basic geometrical properties of the specimens. The specimens consist of ten stubs with eight stiffened specimens and two non-stiffened counterparts. The cross sections of the specimens with stiffeners are showed in Fig.1. The longitudinal arrangement of stiffeners on steel tubes is showed in Fig.2.

The depth b and length L of all the specimens are 200mm and 600mm respectively. Two nominal steel plate thicknesses t (2.0mm and 3.5mm) were chosen for steel tubes and hot-rolled plate. Reinforcements with nominal diameter d and tensile strips with cross-sectional dimensions $d_r \times t_r$ were employed as stiffeners. Based on the nominal steel plate thickness t, the specimens are divided into two groups: group I (t=2.0mm and corresponding depth-to-thickness ratio b/t=100) and group II (t=3.5mmand corresponding depth-to-thickness ratio b/t=57). In Table 1, α_s is the ratio of steel tube cross-sectional area A_s to concrete cross-sectional area A_c; α_r is the ratio of reinforcement volume V_r to concrete volume V_c The details of the stiffeners in the same stiffened scheme are described in groups as follows:

S1 and S5: non-stiffened specimens, shown in Fig. 1(a), designed as referential specimens.

S2 and S6: stiffened specimens with battlement-shaped reinforcements, shown in Fig.1 (b) and Fig.2 (a). The battlement-shaped reinforcements were made through bending straight reinforcements and welded tangentially on the inner surface of the steel tube. The stiffeners were expected to restrain the tube at the welds and the battlement shape guarantees embedment in concrete. During fabricating the stiffened specimens, the steel plates were folded into L shape, the

inner sides of which were welded with reinforcement stiffeners. Then two L-shaped parts were welded to form a hollow square tube. This fabrication procedure reduced adverse influence caused by welding residual stress compared to traditional workmanships.

S3 and S8: stiffened specimens with oblique battlement-shaped reinforcements, shown in Fig.1(c) and Fig.2 (b). The battlement-shaped reinforcement was positioned near the corners of the tube and welded tangentially to the inner surfaces of the two adjacent steel plates. The weld divided the steel plate cross section into three parts with widths of 65mm, 70mm, and 65mm respectively. An oblique battlement-shaped reinforcement was welded between two adjacent plates, therefore square steel tube should be formed before stiffener welding.

S7: stiffened specimen with welded circular stirrups, shown in Fig.1 (d) and Fig.2(c). Six circular stirrups were welded uniformly-spaced along the length onto the inner surfaces of the steel tube. The stirrups were expected to confine the concrete core and restrain the possible outward deformation of the encasing steel at the location of welds. A circular stirrup was welded on four plates, therefore square steel tube formation should be prior to stiffener welding.

S4, S9 and S10: stiffened specimens with tensile strips, shown in Fig.1 (e) and Fig.2 (d). The tensile strips, with cross-sectional dimensions of 20mm (height) × 2.0mm (thickness) or 20mm (height) × 3.5mm (thickness), were installed through the pre-fabricated holes with dimensions slightly larger than those of the stiffeners. The tensile strips were then welded at two ends, with the spacing of 100 mm along the length. The steel tensile strips were made of the same steel plates of the tubes. This hole-drilling fabricating method can avoid heat-induced initial imperfection by traditional gas-cutting method.

After fabrication of the stiffened tube, an end plate was welded at the bottom for subsequent concrete casting procedure. Accordingly, another end plate was welded to seal the top end of the

specimen after concrete casting procedure. Four steel end ribs with dimensions of 50mm×20mm×2mm were welded at each end of the tube to reinforce the tube's end regions.

2.2 Material properties

According to the Chinese National standard, Metallic materials-tensile testing at ambient temperature (GB/T 228-2002) [12], mechanical properties of the steel plates and stiffeners were tested as it shown in Table 2. Commercial ready-mixed concrete of C30 grade in the Chinese national code for design of concrete structures (GB50010-2010) [13], was casted into hollow tubes, with mix design shown in Table 3. Prismatic standard cubes with dimensions of 100mm×100mm×100mm were casted simultaneously under the same curing conditions. Test specimens were cured until the testing day and the cubes were tested to get the equivalent value of concrete compressive prismatic strength f_{ck}=37.5N/mm^2.

The experiment was carried out at the Structural and Seismic Test Research Center, Harbin Institute of Technology. A 500 ton computer monitored OSD hydraulic jack was used as loading device, with two articulated rigid loading pads at the top and bottom. During the loading procedure, the bottom pad lifted the specimen and the top kept still (shown in Fig. 3).

The axial load was measured with a load cell on the top endplate and a 20mm-thick padding plate was placed in between the load cell and the specimen in order to get evenly distributed axial loads. Two accessory columns, with retractable length, were specially designed to support the top loading pad along with the specimen, in order to stably record the load-displacement curves during load descending stage (Fig. 3). Four LVDTs (1,2,3 and 4)were placed at bottom and two (5 and 6 in parenthesis)were at top (Fig. 3(c)), so relative vertical displacement u_r after the specimen and devises were close-contact, is calculated with Eq. (1):

$$u_r = u_b - u_t \tag{1}$$

Where u_b is the average data value of the bottom four sensors; u_t is the average data value of the top two sensors. The data from the load cell and LVDTs were input into the Beijing spectrum instrument so that the axial load-displacement curves were real-time monitored.

Four dial gauges were symmetrically arranged with starting gage length 20mm in the middle of each steel plate (in Fig.3(c)), for measuring displacement increment prior to local buckling. Vertical and transverse strain gauges were also employed on the tubes for monitoring the strain and stress development of non-stiffened specimens and stiffened specimens. To assure uniform compression, preliminary tests within the elastic range were conducted by carefully adjusting the position of the specimen, based on the data of the dial gauges and strain gauges. The dial gauges and strain gauges were used for displacement and strain measurement, and for physical centering adjustment before actual loading.

A load increment of less than one tenth of the estimated peak resistance was employed in the loading scheme. Each load interval was maintained for about 2 minutes.

2.4 Test observation

2.4.1Buckling behavior of steel tubes

Figures 4-7 illustrate the buckling modes of steel tubes of specimens S1, S4, S5 and S9, which are typical specimens in their groups. Specimens S1 and S5 are both non-stiffened counterparts. The comparison is designed to investigate the influence of tube thickness t, in other words, depth-to-thickness ratio b/t. Specimens S4 and S9, both tensile strip stiffened specimens with tube thickness respectively equal to those of S1 and S5, are studied to investigate influence of tensile strip stiffener on the buckling behavior. The buckling formation time is denoted with load values or loading stages at the buckling positions of the steel tubes.

Table 4 lists the buckling load P_b when tube buckling was first observed, the yielding load P_y

when steel tube yielding occurred, the ultimate load P_u and the classification of composite sections. The tube buckling here is referred only to the cross-sectional buckling in the middle of the tube, where the buckling is only influenced by cross-sectional slenderness and concrete support. This is different to the end tube's buckling which is caused by end concrete shrinkage resulting in the end tube bearing the axial load prior to the concrete core. Before reaching the point of yielding load corresponds to steel tube yielding, the interaction between concrete and steel tube can be ignored. Therefore, the uniaxial stress-strain relation curves of concrete and steel are employed to calculate the yielding resistance.

Test results show that the stiffeners help to increase the buckling resistance of columns. The depth-to-thickness ratio (b/t =100) of specimen S1 is beyond the limits in Euro code 4 (EN1994-1-1: 2004) [14] in which the effects of local buckling can be neglected. Due to its flexible cross-sectional slenderness, the specimen S1 buckled at 600kN before reaching its yielding resistance of 1900kN. The composite section of S1 belongs to Class 4 grade according to the rule of cross-section classification in Euro code 4. By adding stiffeners in specimens S2, S3, and S4, the buckling was delayed and their buckling loads (respectively 1000kN, 1200kN and 1200kN) are relatively closer to yielding load (1900kN).

Although the depth-to-thickness ratio (b/t=57) of Specimen S5 is beyond the limits in Euro code 4 in which the effects of local buckling can be neglected, specimen S5 buckled at 2500kN after its tube reached yielding resistance 2211kN in the experiment. Compared to specimen S5, no buckling was developed in specimens S6, S7, S8, S9, and S10, which failed by material failure beyond peak resistance, rather than local buckling failure in elastic and plastic stage. It can be indicated that, without thickening the tubes, the stiffeners further upgrade classification of composite sections to Class 2 grade, in which the cross sections can develop their limited plastic resistances and

deformation because of local buckling.

2.4.2Mechanical behavior of stiffeners

The buckling behaviors of specimens can be attributed to stiffening mechanisms, in which the stiffeners delay the local buckling and almost fully restrain the out-of-plane deformation of steel tubes at the location of welds. The results deduced from experiment on the tubes' buckling modes and stiffeners' mechanisms not only confirm the conclusions of the author's previous experiment [1], but also investigate new stiffeners' mechanisms and more comprehensively summarize the common mechanisms among different stiffeners. The mechanisms of stiffeners in this experiment are described as follows.

The steel tubes of non-stiffened specimens S1 and S5 supported loads independently and buckled outward in very early stage, due to little interaction with concrete. The buckling wave heights of specimens S1 and S5 were significant, with 15~20mm and 10~15mm respectively. Without lateral restrain from concrete, the steel tubes lost their resistances rapidly during load descending stage and steel material capacity are far from fully exploited.

The adverse buckling behavior in the non-stiffened specimens was noticeably improved by stiffeners in the stiffened specimens. For specimens S2 and S6 (shown in Fig.1 (a),(b)), the segments of the battlement-shaped reinforcements, vertical to steel plates, effectively restrained the tube at welds in order to change tube's buckling modes and increase its buckling strength. On the other side, the battlement-shaped reinforcements were embedded in the concrete and the concrete expansion deteriorated stiffeners' boundary condition, which slightly decreases specimens' behavior. The buckling wave heights of specimens S2 and S6 were in the range of 5~10mm and 0~5mm respectively.

Specimens S3 and S8 have stiffeners arranged obliquely at two adjacent steel plates. The smaller

spacing of welding constraint points in cross section provided more uniformly distributed lateral confinement for concrete. Meanwhile, the horizontal segments of the battlement-shaped reinforcements directly restrained the out-of-plane deformation of the tubes at welds. The buckling wave heights of specimens S3 and S8 were respectively mainly 5~10mm and 0~5mm.

In the specimen S7, the circular stirrups offered some direct confinement for concrete and the tube stiffened by circular stirrups at welds offered another kind of confinement. The buckling wave heights of specimen S7 were only 5~10mm.

Specimens S4, S9, and S10, employing tensile strips, restrain out-of-plane deformation of steel tubes at location of welds. The strips helped steel tube restrain concrete expansion and provide confinement for concrete. The buckling wave heights of specimens S4, S9 and S10 were only 0~10mm.

2.4.3 Concrete crushing and failure modes

Local concrete crushed mode (as surface 3 of specimen S5 shown in Fig.8 (c)) was observed in the concrete in the non-stiffened tube. But most other concrete surfaces were detected crushed only to a shallow depth (as surface 1, 2 and 4 shown in Fig.8 (a), (b) and (d)), which means the compressive strength of most concrete was not fully exploited. After premature local buckling of the steel tube due to the lack of stiffeners' restraint, little confinement from the steel tube was provided for the concrete core. The concrete was loaded to crush very rapidly and can be regarded as brittle failure mode. The interaction between concrete and steel tube can also be detected by tapping the buckling locations of the steel tube after experiment, for the tapping sound revealed that there was separation between the concrete and steel tube.

The concrete in the stiffened tubes (such as S9 in Fig. 9) was damaged in local concrete crushed mode, i.e. no obvious diagonal cracks but local concrete trivial cracks and crush, which means the

compressive strength of concrete was exploited. The crushed area and crushed depth were more than those of the non-stiffened specimen. The crushed concrete was located between two adjacent stiffener welds, while concrete near welds showed little damage. The interaction between concrete and steel tube can also be detected by tapping the buckling locations of the steel tube after test, for the tapping sound revealed that there were almost no separation between concrete and steel tube. The stiffeners enhance the constraint effect for concrete provided by steel tube and improve the concrete from a brittle failure mode to a more ductile failure mode.

2.5 Comparison of experimental results

The axial load P versus axial shortening u relation curves of all the specimens were recorded in the experiment. The axial shortening u of the specimens was obtained by modifying the displacement transducer readings on the basis of the vertical strain gauge and dial gauges readings to eliminate the shortening caused by loose contact of devises. The quantifications of axial stress-strain relation curves, defined as derived behavioral indices, are summarized in Table 6. Comparisons and analysis of mechanical properties of all specimens are conducted as follows, combined with the results in Fig.10 and Table 5.

In Table 5, the indices P_{n} and P_{u} are nominal ultimate resistance and test ultimate resistance. P_{n} can be referred to author's previous paper [1]. The P_{u} from tests is the peak resistance of P-u relation curves, which was influenced by steel tube stiffening and concrete confinement, in other words, the positive interaction between concrete and steel tube. To eliminate the differences of sectional dimensions and tube thicknesses among specimens, the test ultimate resistance enhancement index (RI) is introduced and defined in Eq.(2).

$$RI = P_u / P_n \tag{2}$$

The ductility factor μ measures deformation capacity of specimens. It can be defined as the ratio

of axial shortening corresponding to 85% ultimate resistance during descending stage $u_{0.85}$ to the yielding axial shortening u_y in Eq.(3). The u_y is the axial shortening corresponding to decrease of slope coefficient of the axial load-axial shortening curve, that is, the materials evolve from elastic stage to plastic stage.

$$\mu=u_{0.85}/u_y \tag{3}$$

To investigate the enhancement of ductility by the stiffeners over that of the non-stiffened specimen, ductility enhancement index *DI* is defined as the ratio of ductility of stiffened specimen to that of non-stiffened specimen.

Based on the data in Table 5, the test ultimate resistance enhancement index RI of all the specimens in the test range from 1.08 to 1.19, which indicates the test ultimate resistances P_u from test are generally larger than nominal ultimate resistances P_n. The reason can attribute to the effective interaction between concrete and steel tubes. The majority enhancement of index RI comes from concrete confinement provided by stiffened steel tubes.

The stiffeners improved specimens' ductility more than ultimate resistance. Compared to non-stiffened counterpart, the stiffeners of tensile strip, oblique battlement-shaped reinforcement and welded circular stirrup can increase the ultimate resistances of Group II specimens only by 3% to 4.5%, While the ductility enhancement by stiffeners can reach up to 46%~77%. That is because the confinement for concrete depends on how much steel tube provide restriction to concrete volume expansion. During load ascending stage (including ultimate resistance), the concrete expansion is very small and the interaction between concrete and stiffened steel tubes can be ignored. During load descending stage, damage in concrete makes its volume expanded quickly and therefore the stiffened steel tubes began to restrict the concrete expansion and provide more effective confinement for concrete. The tensile strip, oblique battlement-shaped reinforcement and

welded circular stirrup can directly restrain the steel plates through the steel tensile capacity and improve specimens in ductility more significantly.

It should be specially mentioned that the tensile strip stiffener of specimen S10 was inadequate in cross section compared to that of specimen S9, and therefore the specimen S10 provided relatively low resistance. The battlement-shaped reinforcement cannot significantly increase resistances of specimens S2 and S6, as its embedment in concrete hampered concrete compressive strength's full exploitation and its restriction of steel plates was a little deteriorated with concrete expansion.

It should be stressed that the steel tubes in this experiment have a steel to concrete proportion α_s of 4.2% ~ 7.5% (shown in Table 1), reaching the lower limit of CFST steel proportions (normal steel proportion range is 4%~20%), which requires lower constructional costs in China. An enhancement in performance may be expected with thicker steel tubes within normal steel proportion range. The amount of stiffeners should coordinate with steel proportion, in order to guarantee their economic usage.

3. Theoretical analysis

3.1 Introduction of numerical analysis model

A numerical analysis program was designed by the authors to perform the numerical analysis of the specimen. The detailed numerical model to underpin the analysis program is introduced in this section.

3.1.1 Axial load-displacement curves of stiffened square CFST stubs subjected axial load

Load-displacement curves of stiffened square CFST stubs were calculated in the numerical model. The numerical model is established by applying axial displacement u on top of columns step by step. Then the axial displacement is divided by column length to be translated into sectional strain. Stress-strain relation curves of constraint concrete and steel tube proposed are employed to

calculate their stresses. In the *ith* loading increment of axial load-displacement curve, and the axial resistance P_i of the columns can be specifically expressed as Eq. (4):

$$P_i=f_{cci}A_c+f_{yi}A_s \tag{4}$$

in which f_{cci} and f_{yi} are stresses of constraint concrete and steel tube. The maximum value of f_{cci} is compressive prismatic strength of constraint concrete; the maximum value of f_{yi} is yield strength or local buckling strength of steel tube. A_c and A_s are cross-sectional areas of constraint concrete and steel tube respectively.

Therefore the axial resistance P and axial displacement u of columns are collected for the load-displacement relation curves. When the axial load descended to 85% of the peak load (the value 85% is larger than most upper limits of axial compression ratio in reinforced concrete tall buildings), the column is considered to be damaged and the iteration procedure stops.

In the numerical analysis, the concrete strength takes into account constraint effect provided by steel tube and distribution of confined concrete. The strength of steel tube considers influence of local buckling. Only CFST stubs are researched in this paper, therefore overall buckling of specimen is ignored. Compaq Visual Fortran language is employed to code the numerical analysis program of stiffened square CFST stubs on axial concentric compressive performance.

3.1.2 Material model of steel plates to simulate the buckling behavior

The main failure mode of the steel tube in CFST stubs subjected to axial load is local buckling. Local buckling was considered in this numerical analysis, which provides more accurate simulation results than author's previous research [1], in which no consideration of local buckling was made.

In non-stiffened CFST specimens, the concrete core can restrict tube inward deformation of the tube which is detected in the hollow tube specimen. Therefore the steel tube can only buckle outward, which means the existence of concrete changes the buckling mode of the steel tube. Figure

11 shows the buckling mode of non-stiffened steel tube in CFST with dotted lines on the basis of finite element analysis conducted by the author. In the test, the steel tube corners are restricted by the concrete corners. Therefore in the analysis the steel plate can be approximately considered as fixed at the corners (shown in Figure 11 (a)). Along longitudinal direction, the steel tube takes on multi-wave buckling mode. The connection of two adjacent buckling waves contacts tangentially to the concrete surface. The steel plate can be approximately supposed to be fixed in rotation at two ends of every buckling wave (shown in Figure 11 (b)), with longitudinal displacement fixed at one end and unfixed at another end. Figure 12 is the simplified model of rectangular steel plate subjected to uni-directionally uniformly-distributed loading. The dimensions of the rectangular steel plate are a (in x direction) and b (in y direction). The line load p_x on neutral surface in x direction represents the axial load on the steel tube. All the edges of the steel plate are restrained in y direction and rotations, with x directional freedom restrained only at edge AD or edge BC.

Although the local buckling of steel tube is inevitable in most cases, the setting of proper stiffeners on inner surfaces of steel tube is an efficient method to postpone local buckling. The stiffeners in this paper employ their tensile capacity by pulling out-of-plane deformation of steel plate at location of welds. The stiffeners can effectively change steel plate from low-order buckling mode into in high-order buckling mode, or even postpone the buckling to plastic stage. The restriction function of stiffeners on steel plate can be approximately simulated with point restriction at location of welds without consideration of concrete expansion.

The elastic buckling strength f'_{cr} (N/mm^2) of steel plates in stiffened CFSTs can expressed as Eq. (5), considering buckling postponing function of stiffeners on steel plates. The Eq. (5) has been compared with finite element analysis results for verifications in Figure 13. The comparison can be mainly accepted when the depth-to-thickness b/t ratio is 20～150, the yield strength f_y is Q235～

Q420 and the numbers of longitudinal or horizontal point restrictions are 0, 1 and 2.

$$f_{cr}^{'} = \alpha_a \alpha_b f_{cr} = \alpha_a \alpha_b \frac{\pi^2 D}{b^2}(4\frac{a^2}{b^2} + 4\frac{b^2}{a^2} + \frac{8}{3}) \tag{5}$$

For square steel plates (a=b), the Eq. (5) can be simplified as

$$f_{cr}^{'} = \alpha_a \alpha_b f_{cr} = 10.67 \alpha_a \alpha_b \frac{\pi^2 D}{b^2} \tag{6}$$

f_{cr} is elastic buckling strength of steel plates in non-stiffened CFSTs [15]. D is the flexural rigidity per unit width and is given by

$$D = \frac{Et^3}{12(1-v^2)} \tag{7}$$

t is the thickness of the steel tube (mm); E is the elastic modulus of steel plate (N/mm^2); v is Poisson's ratio of steel plate taken as 0.287.

α_a and α_b are influence coefficients, respectively considering longitudinal spacing S_a and horizontal spacing S_b of adjacent stiffener welds, expressed as Eq. (8) and (9).

$$\alpha_a = \sqrt{\left(\frac{S_a}{a}\right)^2 + \left(1 - \left(\frac{S_a}{a}\right)^2\right)\frac{f_y}{f_{cr}}} \tag{8}$$

$$\alpha_b = \sqrt{\left(\frac{S_b}{b}\right)^2 + \left(1 - \left(\frac{S_b}{b}\right)^2\right)\frac{f_y}{f_{cr}}} \tag{9}$$

where a and b are in-plane dimensions of single buckling wave of non-stiffened steel plate. a is longitudinal distance between wave crests of adjacent buckling waves; b is cross-sectional length of steel plate.

The uniaxial perfect elastic-plastic model (shown in Fig.14) was adopted as the constitutive relationship of material in steel tube and reinforcement, with Young's modulus E_s respectively referring to Table 2. For stiffened specimens, if elastic buckling strength $f_{cr}^{'}$ is smaller than yielding strength f_y, local buckling will occur before attainment of yielding stress in one or more

plates of steel cross-section, and $f_{cr}^{'}$ is employed instead of f_y in the steel constitutive relationship and in the equation (4). If $f_{cr}^{'}$ is equal to or larger than f_y, local buckling will occur beyond the yielding point and one or more plates of steel cross-section can be assumed a plastic stress distribution. Then f_y is used in the steel constitutive relationship. Similarly, this calculation method is also suitable for non-stiffened specimens.

3.1.3 Concrete material model

As per previous research, the concrete in square CFST is divided into a constraint region and non-constraint regions. The non-constraint concrete is described with uni-axial stress-strain relation curve of plain concrete referred to GB50010-2002 or author's previous published paper [1]. The constraint concrete employs the modified Mander concrete model (in Fig.15) proposed by Mander, Priestley and Park in 1988 [16].The favorable influence of transverse confinement on the axial stress-strain relation is taken into consideration in the constraint concrete.

Related research reveals that, in non-stiffened square CFSTs (S1 and S5), cross-sectional constraint region (shaded area in Fig. 16) distributes near the corners of composite tube and the center of concrete, and carries out transition to the non-constraint regions (blank areas) adjacent to the steel plate center (in Fig. 16(a)). For these stiffened specimens, the stiffeners restrain steel tube's local buckling at welds, thus the number and location of the welds influence the constraint region. The boundaries between non-constraint regions and constraint region are described by second-order parabola curves. Fig.16 (b)(c)(d) displays the constraint region (shaded area) and non-constraint regions (blank areas) in stiffened cross section of specimens. Fig.17 shows longitudinal distribution of concrete constraint region (shaded area) and the non-constraint regions (blank areas). Section 1-1 is the stiffened cross section in which stiffeners are welded with the steel tube; Sections 2-2 is the weakest cross section between two adjacent stiffened cross sections. Detailed calculation method

can refer to author's previous research [1].

The confinement distribution pattern may vary with parameters of specimens changing. Simplification made in this paper is proved to be accurate in the following test verification. Further study is still requested, especially when specimens' parameters are beyond the scope of this paper.

On the basis of constraint concrete distribution, the compressive strength of constraint concrete f_{cc} and its uni-axial stress-strain relation curve can be obtained by modifying Mander concrete model, which can be referred to author's previous published paper [1]. The constraint region employs uni-axial stress-strain relation curve of constraint concrete and the non-constraint region employs uni-axial stress-strain relation curve of non-constraint concrete.

3.2 Verification of numerical program

A numerical analysis program was coded to simulate the ten specimens in axial load P versus axial shortening u relationship curves (shown in Fig.18). A fairly good agreement is achieved in the initial stiffness, ultimate strength and ductility between the test and simulation.

Comparison was made in terms of ultimate resistance between predicted results P_p and test results P_t of 65 specimens from Han [5], Cai [7], Huang [9], Chen [10], Yang [17], and Yang in this paper, displayed in Fig.19. The cross-sectional depth b ranges from 130mm to 300mm; the thickness of steel tube t from 1.25mm to 12mm; the depth-to-thickness ratio b/t from 37.5 to 240; the steel strength f_y from 162N/mm^2 to 382N/mm^2; the concrete strength f_{ck} from 23.94N/mm^2 to 54.8N/mm^2. The mean value and standard deviation of the ratio of predicted ultimate resistance to test result are respectively 0.999 and 0.08, which illustrates that numerical predicted results have a good agreement with the test results.

3.3 Parametric analysis

An extensive parametric analysis of tensile strip stiffened CFST specimens based on the

numerical model was conducted to investigate influence of the parameters, such as depth-to-thickness ratio b/t (ranging from 200 to 20 when t from 1mm to 10mm), concrete compressive strength f_{ck} (ranging from 20.1MPa to 50.2MPa, accordingly from C30 grade to C80 grade)，yielding strength of steel tubes f_y (ranging from 235MPa to 420MPa, accordingly from Q235 grade to Q420 grade in the Chinese national code for design of steel structures (GB 50017-2003) [18]), longitudinal spacing of stiffener welds S_a (ranging from 25mm to 200mm), horizontal spacing of stiffener welds S_b (ranging from 25mm to 200mm), thickness of tensile strips t_r (ranging from 2mm to 8mm) and yielding strength of stiffeners f_{yr} (ranging from 235MPa to 420MPa, accordingly from Q235 grade to Q420 grade). In each simulation case, except for the concerned parameter, the remaining parameters are taken as constants, i.e. L=600mm, b=200mm, t=2mm, f_{ck}=26.8MPa, f_y=345MPa, d_r=20mm, t_r=2mm, S_a=100mm, S_b=100mm and f_{yr}=345MPa.

Fig.20 shows the influence of parameters mentioned above on the axial load P versus axial shortening u curves of stiffened specimens and on the ultimate load P_u. It can be seen that the decrease of depth-to-thickness ratio b/t brings significant increase in ultimate load and ductility (Fig.20 (a)). The increasing trend of ultimate load P_u is more obvious when the depth-to-thickness ratio b/t is smaller than 50, for tubes with thickness of more than 4mm, local buckling can be avoided and they also provide more effective constraint effect for concrete. The increase in concrete strength f_{ck} brings linear growth of ultimate load, however, the brittle concrete of high strength makes ductility drop (Fig.20 (b)). As expected, the increase of yielding strength of steel tubes f_y brings linear growth of ultimate load and ductility (Fig.20 (c)). Closer longitudinal and horizontal spacing of adjacent stiffener welds also promotes higher ultimate resistance, for the improved confinement for concrete core, thus providing more economical efficiency of materials. However, when longitudinal and horizontal spacing of stiffener welds both decreases to 100mm, the

improvement of confinement can be ignored (Fig.20 (d) (e)). In regard to construction procedure, fabrication difficulties may arise when spacing of adjacent stiffener welds is too small. Therefore the optimum spacing S_a and S_b are suggested to be 100mm (that is the 1/2 of cross-sectional dimension b). Thickness of tensile strips t_r presents positive influence on ultimate load and ductility (Fig.20 (f)), for the lateral stress of concrete benefits from the axial force of tensile strips. The tensile strip with large thickness brings high ultimate resistance and ductility. Moreover, even very thin tensile strip can effectively improve mechanical behavior of specimens. Therefore, the tensile strip is suggested to have the same thickness with the steel tube, as long as the welding requirements are satisfied. In addition, the yielding strength of stiffeners f_{yr} has little influence on ultimate load and ductility (Fig.20 (g)).

4. Conclusions

(1) The stiffeners proposed in this research help to delay or even prevent local buckling of steel tubes. For specimens with steel depth-to-thickness ratio of 100, the buckling loads of stiffened specimens are increased closer to their yielding loads. For specimens with steel depth-to-thickness ratio of 57, the plastic resistance of stiffened specimens can be developed without considering the effect of local buckling of steel tubes. The stiffeners enhance the constraint effect for concrete provided by steel tube and improve the concrete from a brittle failure mode to a more ductile failure mode.

(2) The tensile strip, the oblique battlement-shaped reinforcement and the welded circular stirrup can directly restrain the steel plates. The stiffeners play little role in specimens' ultimate resistance but can improve ductility by 35% to 126% compared to non-stiffened specimens.

(3) A numerical modeling program was developed incorporating the effect of the stiffeners on postponing of tube local buckling and the confinement of the tube. The program was verified with

related experimental data and good accuracy was achieved, therefore it can be used to predict the mechanical behavior of square stiffened CFSTs.

(4) Parametric analysis based on the numerical model shows that the decrease of depth-to-thickness ratio, the increase of concrete compressive strength and steel tube yielding strength, the decrease of horizontal and longitudinal spacing of stiffener welds and the increase of tensile strip thickness all enhance the mechanical behaviors such as resistance and ductility. （问题7）The optimum spacing S_a and S_b are suggested to be 1/2 of cross-sectional dimension (in this paper is 100mm). The tensile strip is suggested to have the same thickness with the steel tube.

Acknowledgements

The project is supported by National Natural Science Foundation of China (51208241) and by Fundamental Research Funds for the Central Universities (lzujbky-2013-m01).

Reference

[1] Wang YY, Yang YL, Zhang SM. Static behaviors of reinforcement-stiffened square concrete-filled steel tubular columns. Thin-Walled Structures 2012; 58: 18-31.

[2] Ge H, Usami T. Strength of concrete-filled thin-walled steel box columns: experiment, Journal of Structural Engineering 1992; 118: 3036-3054.

[3] Kwon YB, Song JY, Kon KS. The structural behavior of concrete-filled steel piers, Proceedings of 16th Congress of IABSE, Lucerne (2000).

[4] Tao Z, Han LH, Wang ZB. Experimental behavior of stiffened concrete-filled thin-walled hollow steel structural (HSS) stub columns. Journal of Constructional Steel Research 2005; 61: 962-983.

[5] Kitada T. Ultimate strength and ductility of state-of-the-art concrete-filled steel bridge piers in Japan. Engineering Structures 1998; 20: 347-354.

[6] Chen Y. Research on static behaviors of new type concrete-filled thin-walled steel tubular columns. Dissertation for the Doctoral Degree in Engineering, Harbin Institute of Technology; 2006. [in Chinese]

[7] Xu C. Experimental study of hysteretic behavior for concrete-filled square thin-walled steel tubular columns. Journal of Constructional Steel Research 2007; 63: 317–325.

[8] Hsu HL, Juang JL. Performance of thin-walled box columns strengthened with internal braces. Thin-Walled Structures 2000; 37:241-258.

[9] Cai J, He ZQ. Axial load behavior of square CFT stub column with binding bars. Journal of Constructional Steel Research 2006; 62: 472–483.

[10] Cai J, He ZQ. Constitutive relationship of square CFT with binding bars. Journal of Engineering Mechanics 2006; 132: 145-150.

[11] Huang CS. Axial load behavior of stiffened concrete-filled steel columns. Journal of Structural Engineering 2002; 128: 1222-1230.

[12] GB/T 228-2002. Metallic materials-tensile testing at ambient temperature. Beijing, China: General Administration of Quality Supervision, Inspection and Quarantine of the People's Republic of China; 2002. [in Chinese]

[13] GB 50010-2010. Code for design of concrete structures. Beijing, China: Ministry of Housing and Urban-Rural Development of China, General Administration of Quality Supervision, Inspection and Quarantine of the People's Republic of China; 2010. [in Chinese]

[14] EN1994-2: 2005. Design of composite steel and concrete structures. Britain: European Committee for Standardization; 2005.

[15] Guo LH, Zhang SM, Kimb WJ, Ranzic G. Behavior of square hollow steel tubes and steel tubes filled with concrete. Thin-Walled Structures 2007; 45: 961-973.

[16] Mander JB, Priestley MJN, Park R. Theoretical stress-strain model for confined concrete. Journal of Structural Engineering 1998; 114: 1804-1826.

[17] Yang ZY. Research on static behavior of square concrete-filled steel tubular stub columns with steel bar stiffeners. Dissertation for the Master Degree in Engineering, Harbin Institute of Technology; 2008. [in Chinese]

[18] GB 50017-2003. Code for design of steel structures. Beijing, China: Ministry of Housing and Urban-Rural Development of China, General Administration of Quality Supervision, Inspection and Quarantine of the People's Republic of China; 2003. [in Chinese]

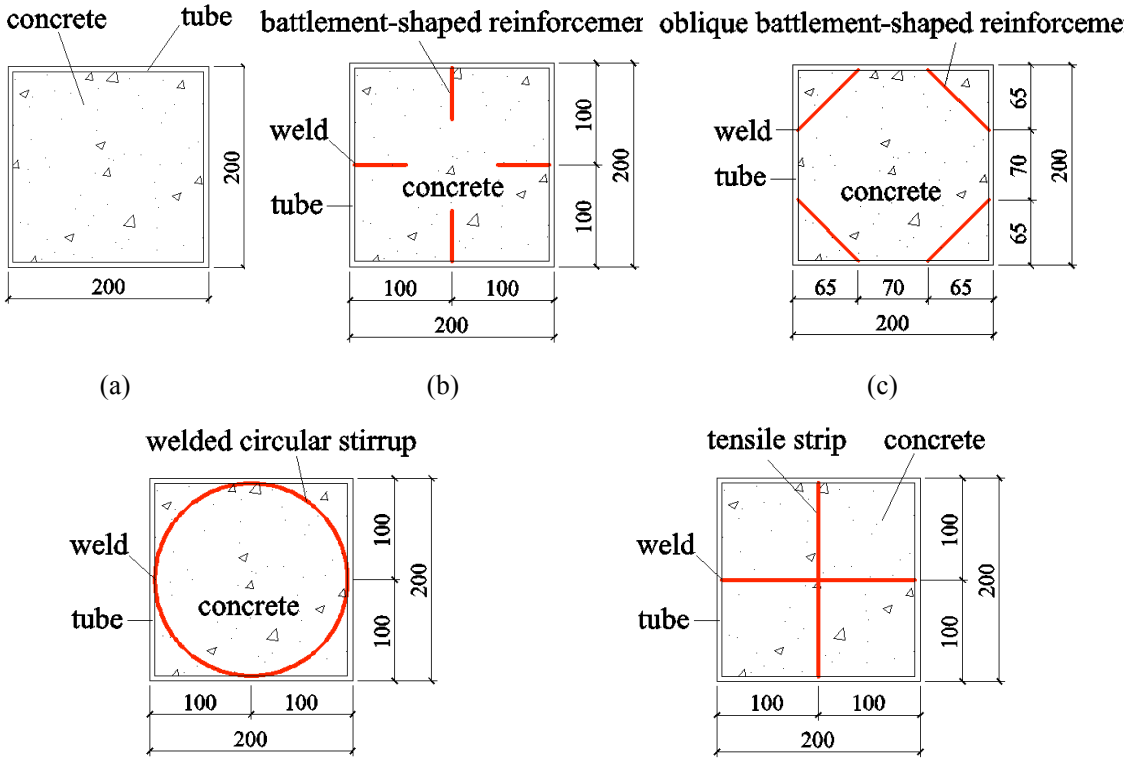

Fig.1 Cross sections of hollow steel tubes with stiffeners (unit: mm)

(a) S1/S5; (b) S2/S6; (c) S3/S8; (d) S7; and (e) S4/S9/S10

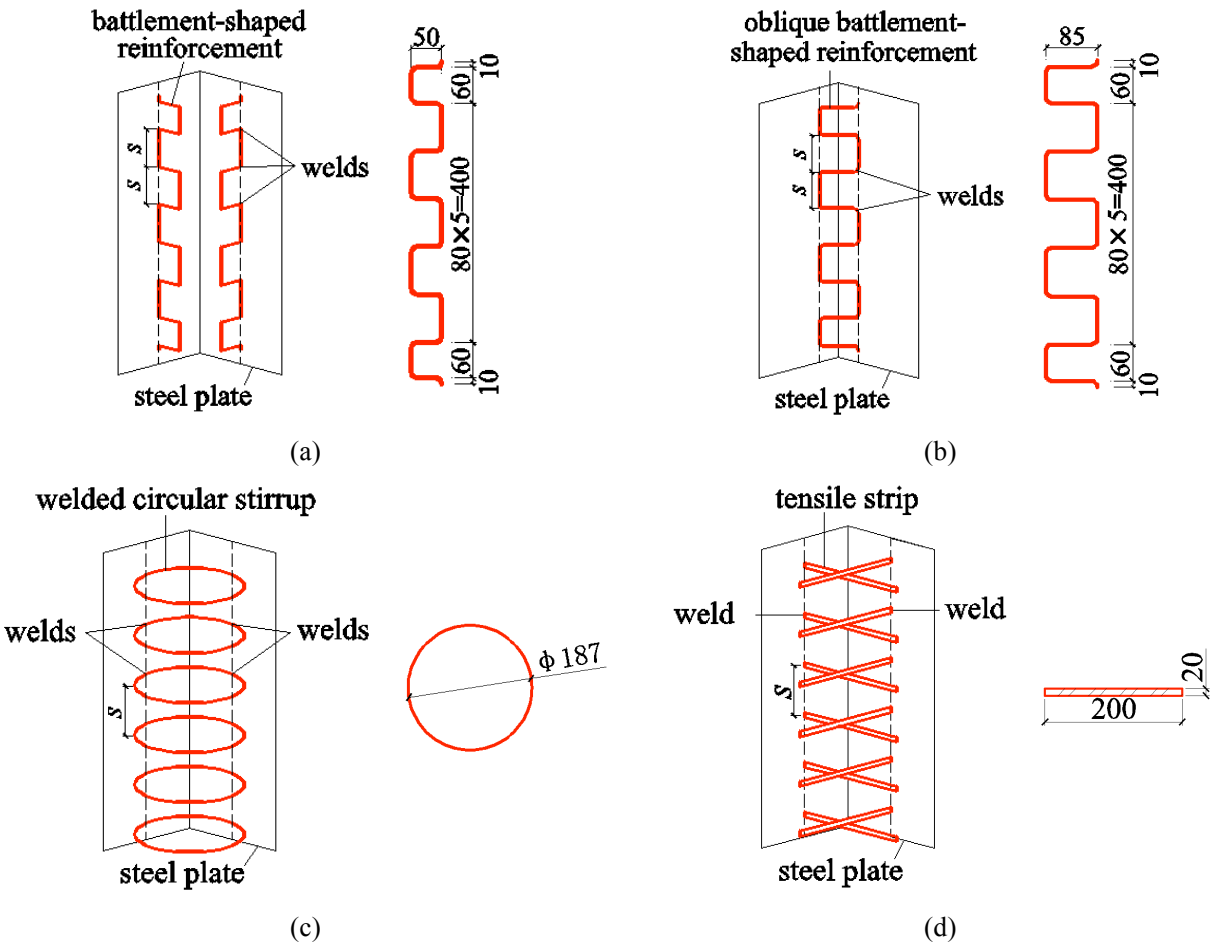

Fig.2 Longitudinal arrangement of stiffeners on two adjacent steel plates (unit: mm)
(a) S2/S6; (b) S3/S8; (c) S7; and (d) S4/S9/S10

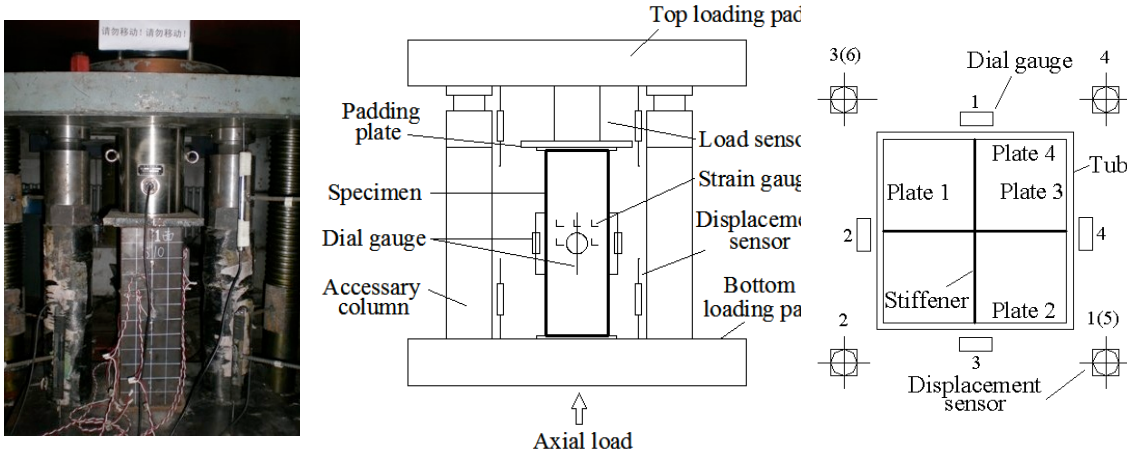

(a) (b) (c)

Fig.3 Loading devices and layout of dial gauges and displacement sensors
(a) Picture of loading; (b) Illustrative drawing of loading; and (c) Measuring apparatus

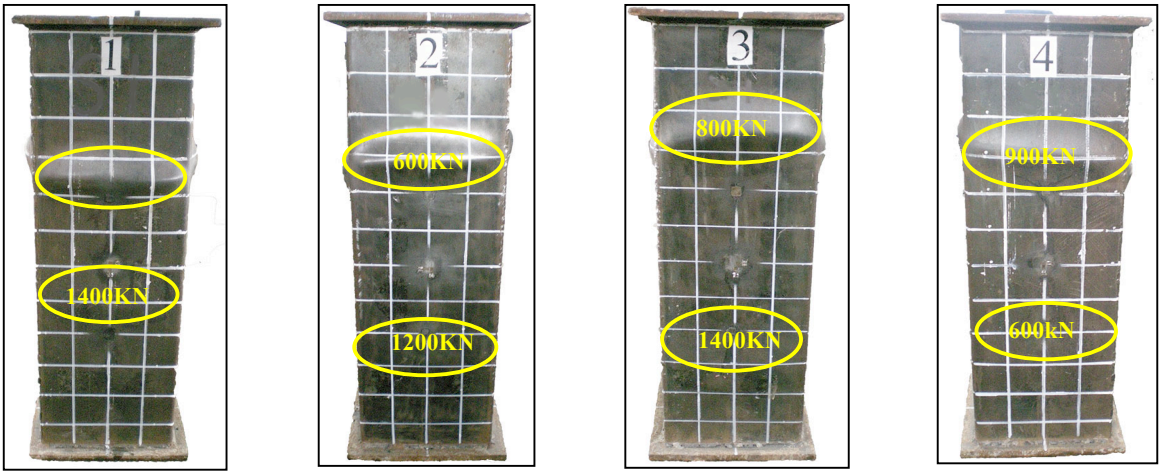

(a) (b) (c) (d)

Fig. 4 Buckling mode of the S1 tube

(a) Surface 1; (b) Surface 2; (c) Surface 3; and (d) Surface 4

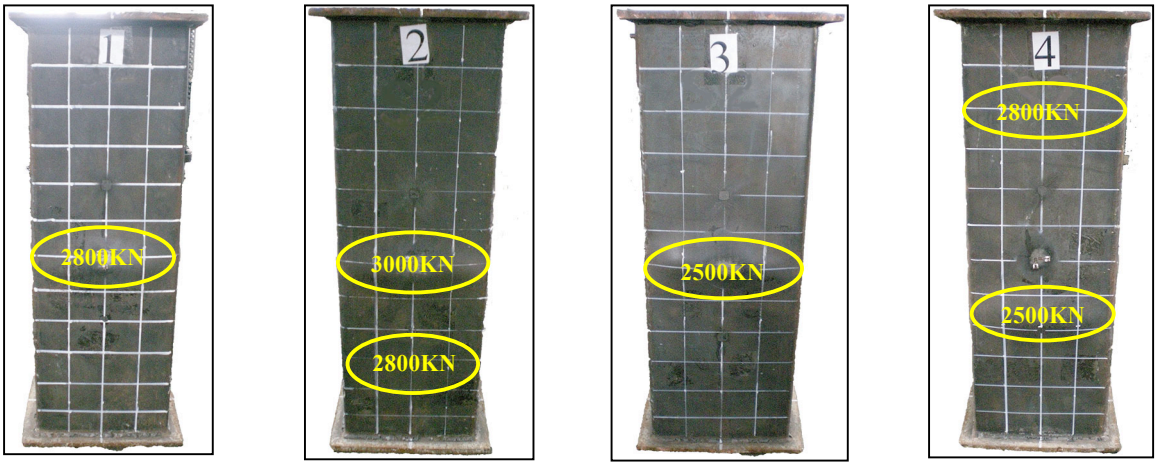

(a) (b) (c) (d)

Fig. 5 Buckling mode of the S5 tube

(a) Surface 1; (b) Surface 2; (c) Surface 3; and (d) Surface 4

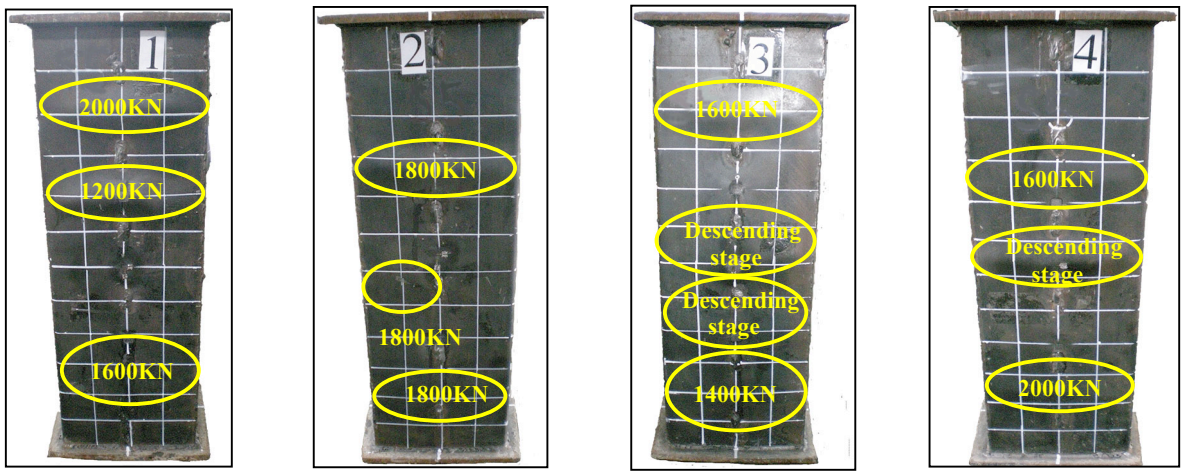

(a) (b) (c) (d)

Fig. 6 Buckling mode of the S4 tube

(a) Surface 1; (b) Surface 2; (c) Surface 3; and (d) Surface 4

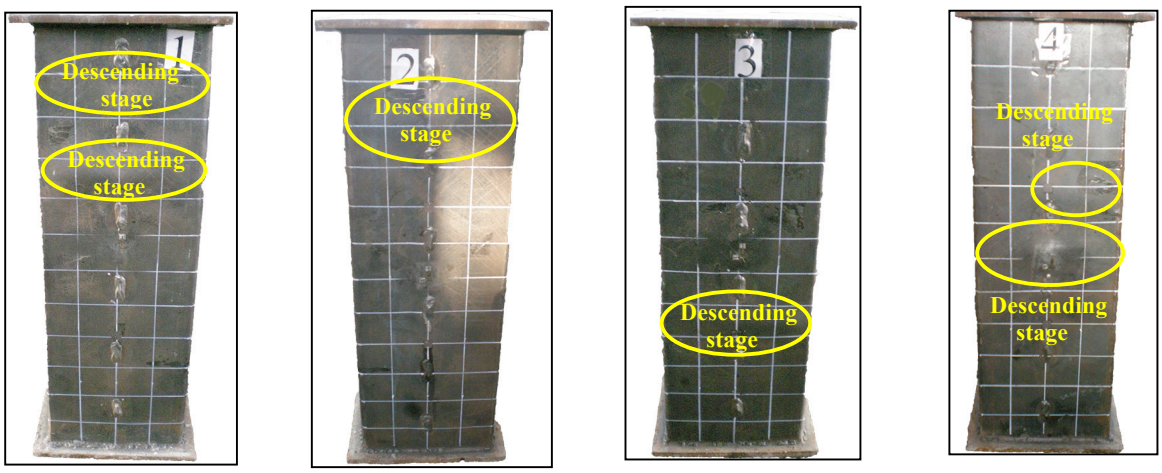

(a) (b) (c) (d)

Fig. 7 Buckling mode of the S9 tube

(a) Surface 1; (b) Surface 2; (c) Surface 3; and (d) Surface 4

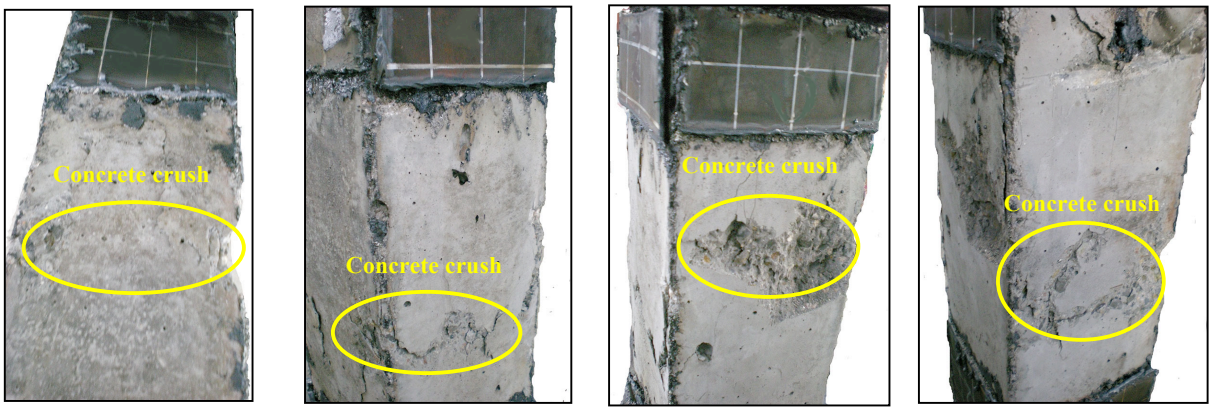

(a) (b) (c) (d)

Fig. 8 Concrete failure mode of the S5 specimen

(a) Surface 1; (b) Surface 2; (c) Surface 3; and (d) Surface 4

(a) (b) (c)

Fig. 9 Concrete failure mode of the S9 specimen
(a) Surface 1; (b) Surface 3; and (c) Surface 4

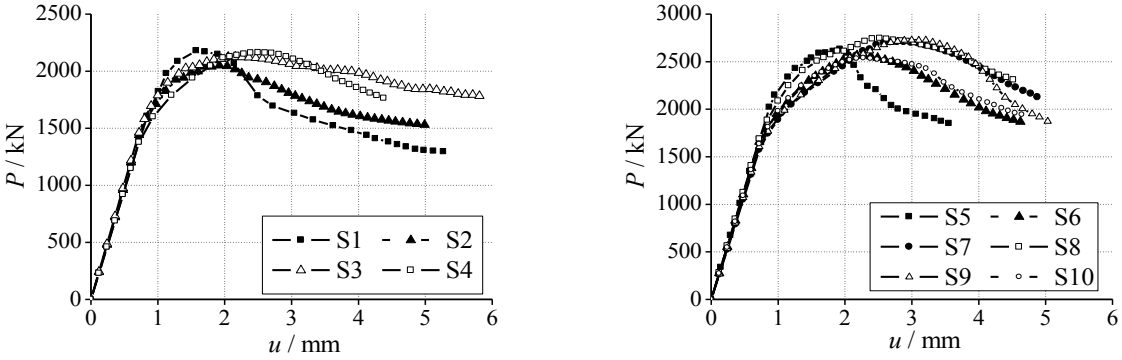

(a) (b)

Fig.10 Axial load-axial shortening relation curves of specimens
(a) Group I (nominal tube thickness is 2.0mm); (b) Group II (nominal tube thickness is 3.5mm)

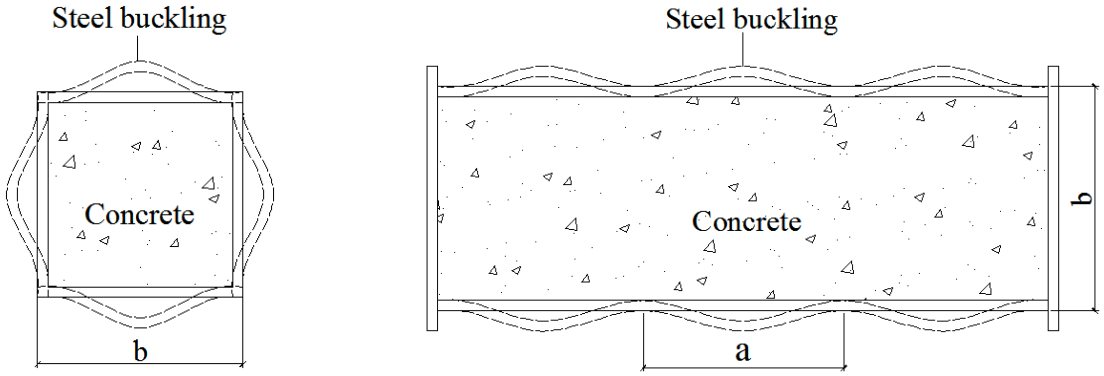

(a) (b)

Fig.11 Boundary conditions of plates in square CFST
(a) in cross sections; (b) along longitudinal direction

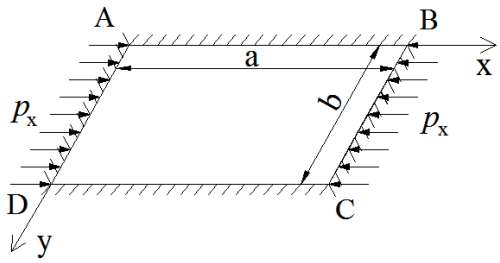

Fig. 12 Four sided fixed plate subjected to uni-directionally uniformly loading

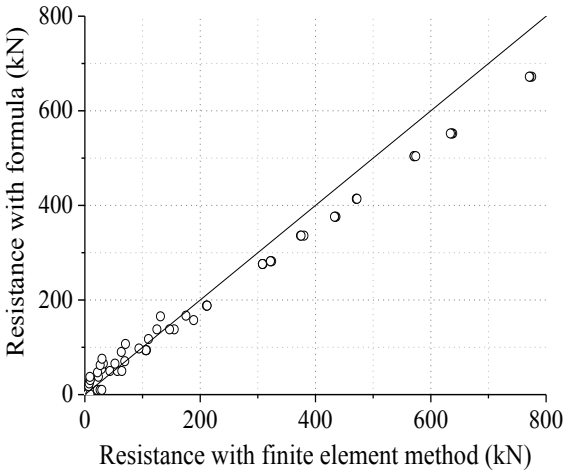

Fig. 13 Verification of formula for elastic buckling strength $f_{cr}^{'}$

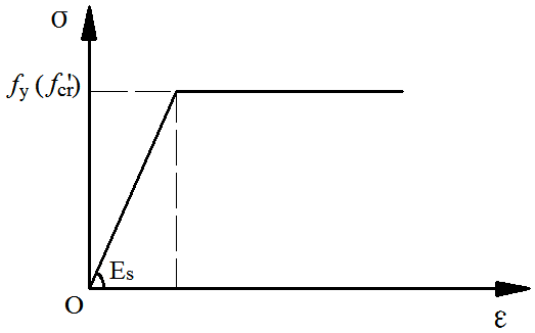

Fig.14 Compressive stress-strain relation for steel tube and reinforcement

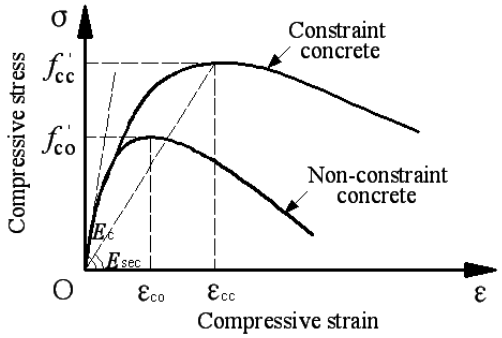

Fig.15 Compressive stress-strain relation for non-constraint and constraint concrete

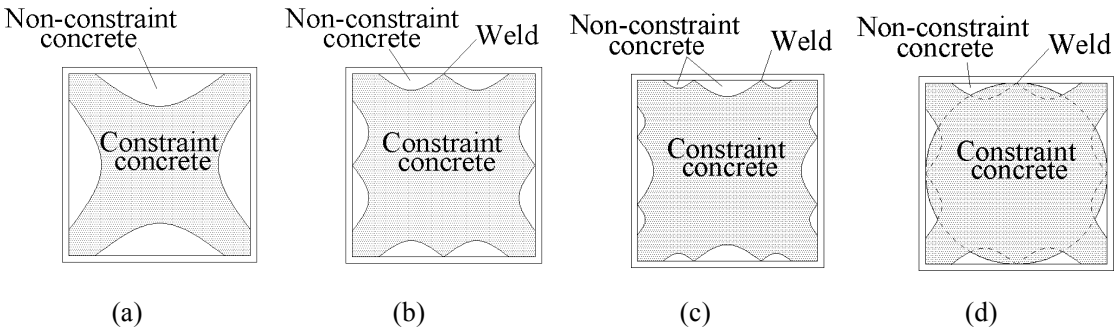

Fig.16 Constraint region of concrete in stiffened cross section
(a) S1/S5; (b) S2/S4/S6/S9/S10; (c) S3/S8; and (d) S7

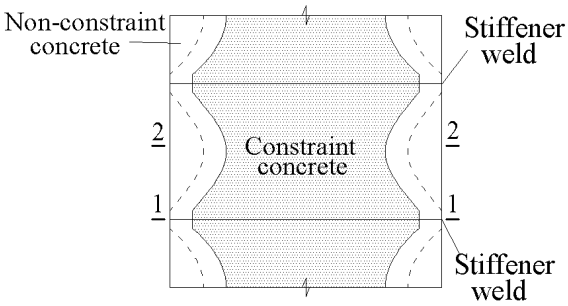

Fig.17 Longitudinal distribution of confinement for concrete

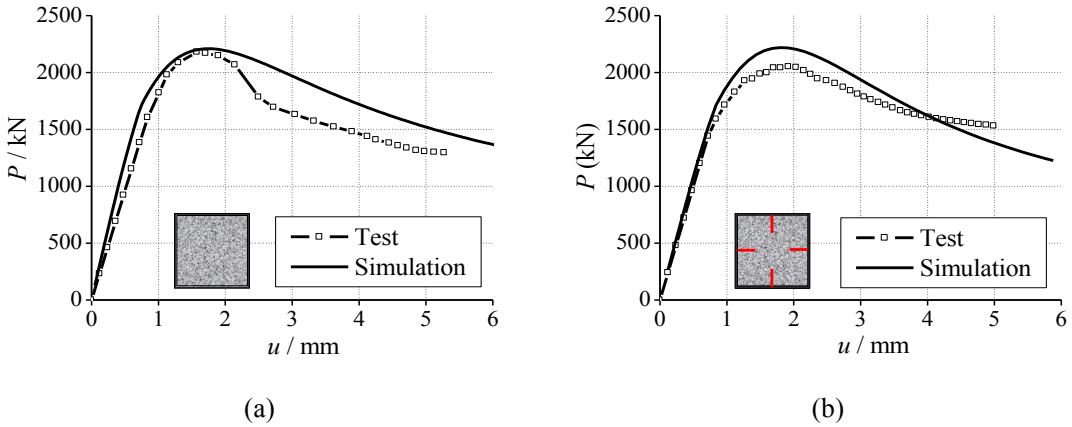

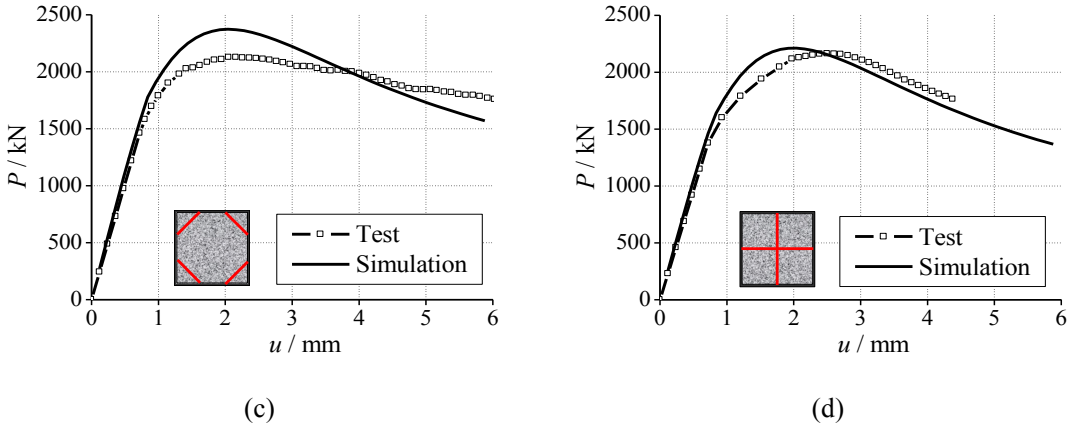

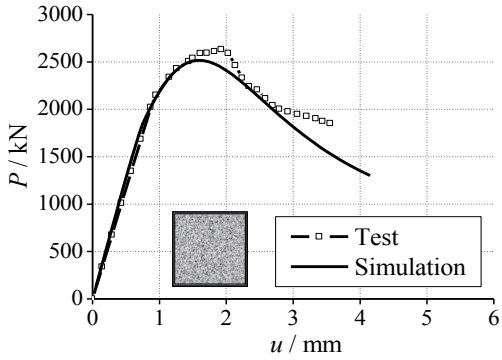

(e)

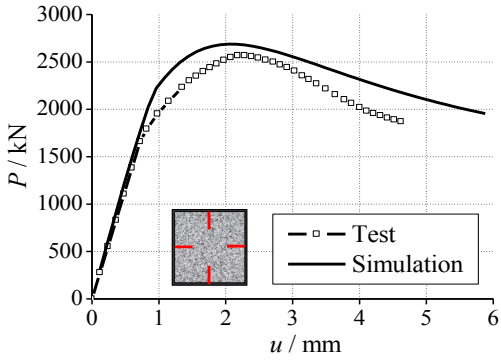

(f)

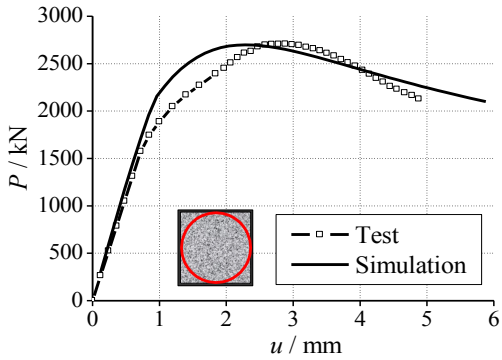

(g)

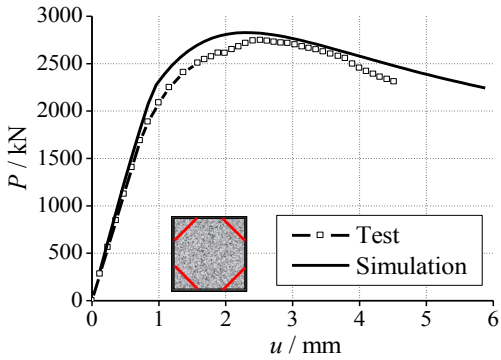

(h)

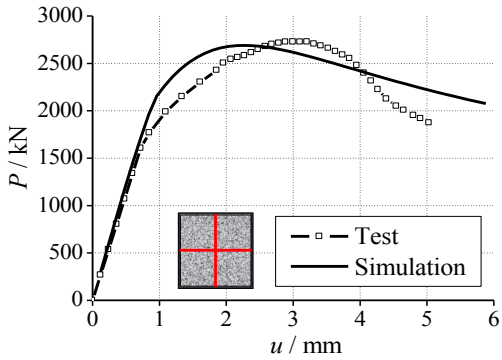

(i)

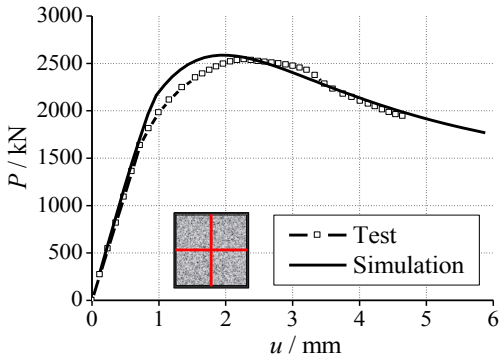

(j)

Fig.18 Comparison of test and simulation results

(a) S1; (b) S2; (c) S3; (d) S4; (e) S5; (f) S6; (g) S7; (h) S8; (i) S9; and (j) S10

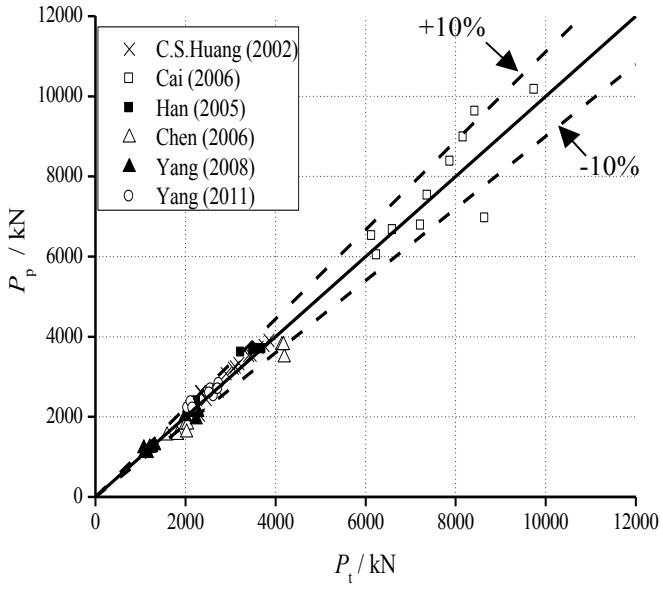

Fig. 19 Comparison between predicted ultimate resistances and experimental ultimate resistances in other scholars' research

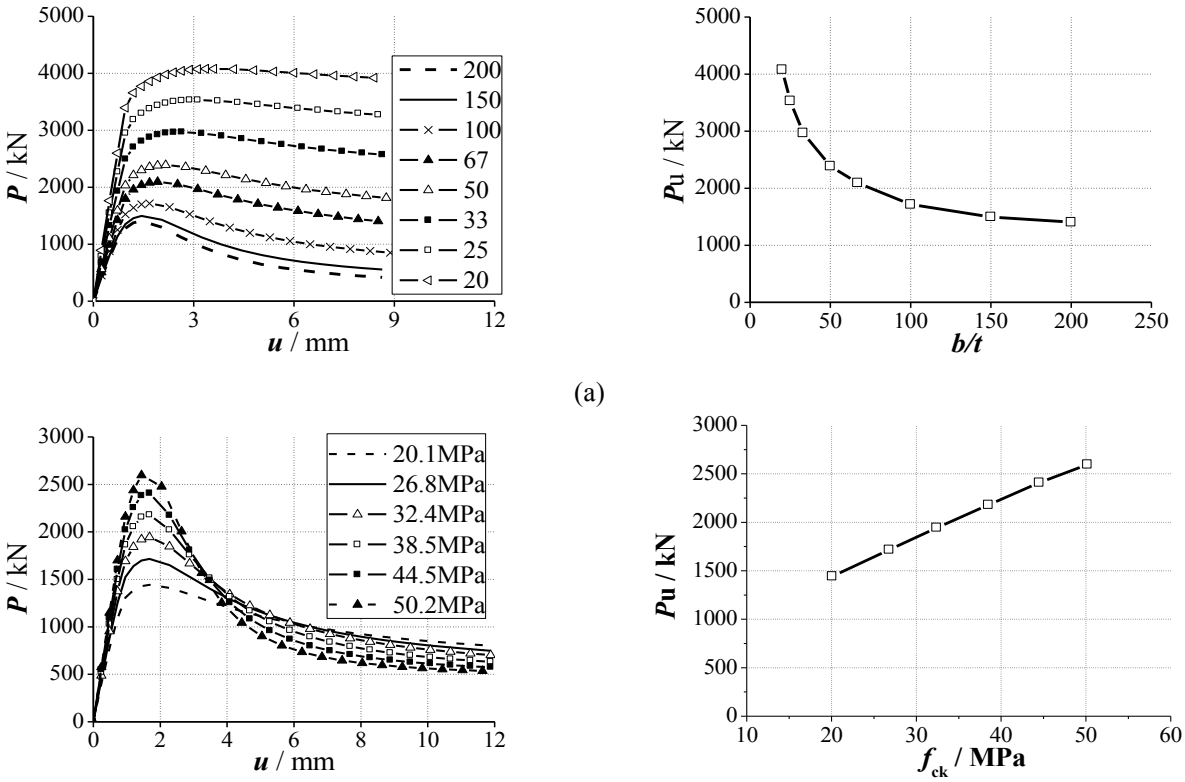

(a)

(b)

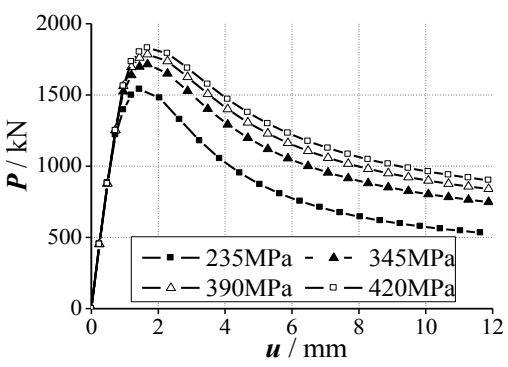
P / kN
u / mm
235MPa
345MPa
390MPa
420MPa

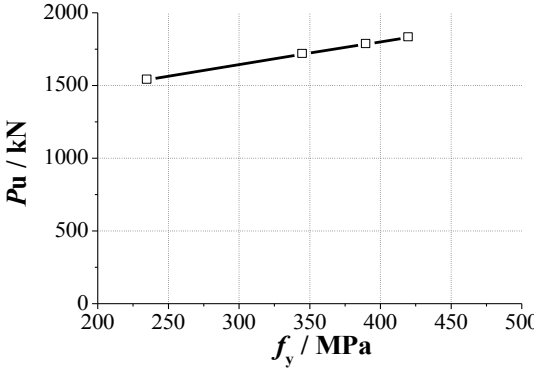
Pu / kN
f_y / MPa

(c)

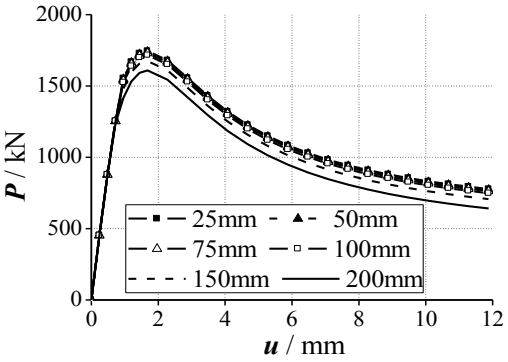
P / kN
u / mm
25mm
50mm
75mm
100mm
150mm
200mm

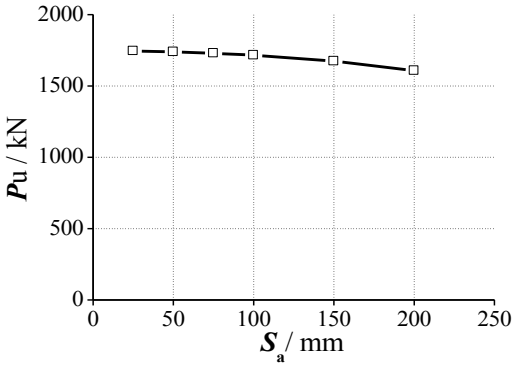
Pu / kN
S_a / mm

(d)

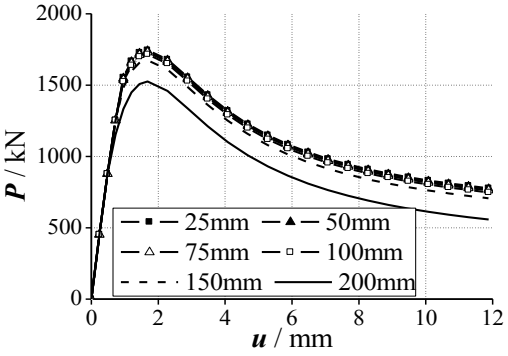
P / kN
u / mm
25mm
50mm
75mm
100mm
150mm
200mm

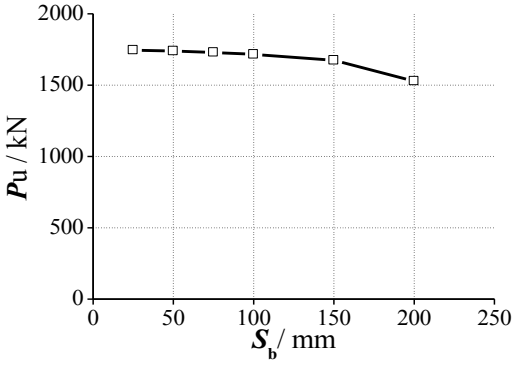
Pu / kN
S_b / mm

(e)

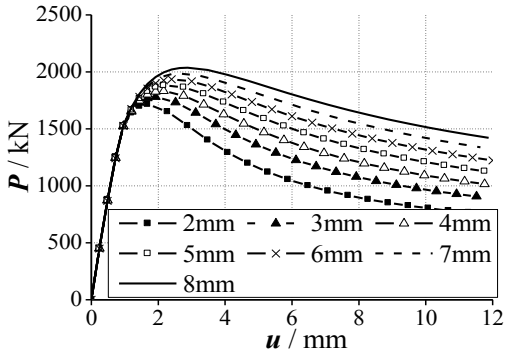
P / kN
u / mm
2mm
3mm
4mm
5mm
6mm
7mm
8mm

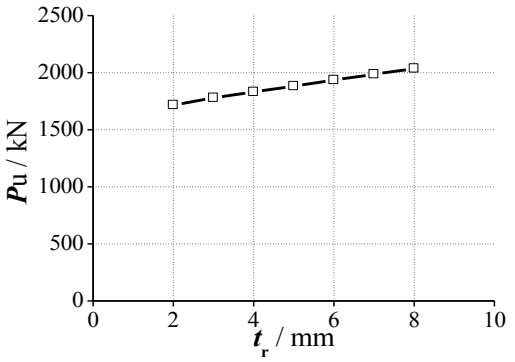
Pu / kN
t_r / mm

(f)

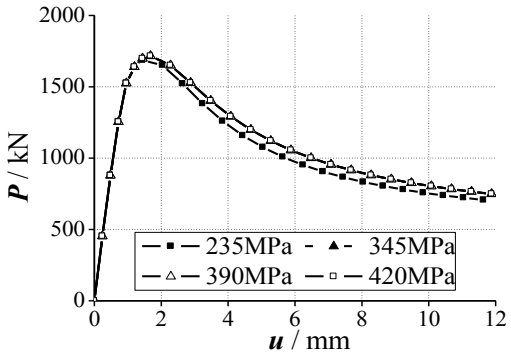

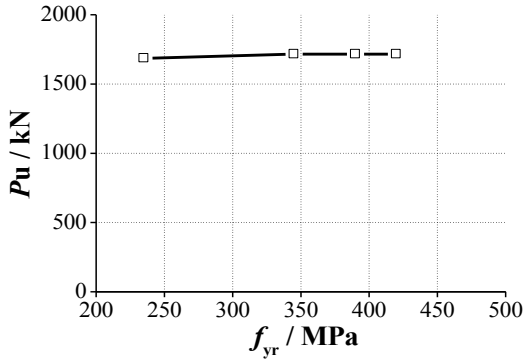

(g)

Fig.20 Parametric analysis

(a) Depth-to-thickness ratio b/t; (b) Concrete strength f_{ck}; (c) Yielding strength of steel tubes f_y; (d) Longitudinal spacing of stiffener welds S_a; (e) Horizontal spacing of stiffener welds S_b; (f) Thickness of tensile strips t_r; and (g) Yielding strength of stiffeners f_{yr}

Table1 Parameters of specimens

Specimen	Stiffener type	Tube thickness t (mm)	Cross-sectional dimension of stiffener $d/d_r \times t_r$ (mm)	Longitudinal spacing of stiffener's welds s (mm)	Steel ratio of tube α_s (%)	Steel ratio of stiffener α_r(%)
S1	None	2.01	—	—	4.2	0
S2	Battlement-shaped reinforcement	1.90	8.0	80	4.2	0.84
S3	Oblique battlement-shaped reinforcement	1.90	8.0	80	4.2	1.08
S4	Tensile strip	1.90	20.0×3.49	100	4.2	0.70
S5	None	3.49	—	—	7.5	0
S6	Battlement-shaped reinforcement	3.49	8.0	80	7.5	0.84
S7	Welded circular stirrup	3.49	8.0	80	7.5	0.86
S8	Oblique battlement-shaped reinforcement	3.49	8.0	80	7.5	1.08
S9	Tensile strip	3.49	20.0×3.49	100	7.5	0.70
S10	Tensile strip	3.49	20.0×2.01	100	7.5	0.40

Table2 Material properties of the steel tubes and stiffeners

Steel pattern	Nominal thickness t (mm)	Nominal diameter d (mm)	Elastic modulus E_s (10^5N/mm^2)	Yield strength f_y (N/mm^2)	Ultimate strength f_u (N/mm^2)
Steel tube I	2.0	—	1.90	301	400
Steel tube II	3.5	—	1.95	315	434
Reinforcement	—	8.0	—	304	463
Tensile strip I	2.0	—	1.90	301	400
Tensile strip II	3.5	—	1.95	315	434

Table3 Mix proportions of concrete (kg/m^3)

Portland cement	Sand	Gravel	Water	Coal ash	Water reducing agent
325	740	1030	185	75	10.4

Table 4 Resistance and classification of composite sections

Group	Specimen	Buckling load P_b (kN)	Yielding load P_y (kN)	Peak load P_u (kN)	Section classification
Group I	S1	600	1900	2185	Class 4
	S2	1000	1900	2051	Class 4
	S3	1200	1900	2127	Class 4
	S4	1200	1900	2163	Class 4

Group II	S5	2500	2211	2630	Class 3
	S6	Exceeding P_u	2211	2567	Class 2
	S7	Exceeding P_u	2211	2706	Class 2
	S8	Exceeding P_u	2211	2746	Class 2
	S9	Exceeding P_u	2211	2726	Class 2
	S10	Exceeding P_u	2211	2538	Class 2

Table 5 Test results

Group	Specimen	Stiffener	P_n (kN)	P_u (kN)	*RI*	μ	*DI*
Group I	S1	None	1920	2185	1.13	1.97	1.00
	S2	Battlement-shaped reinforcement	1894	2051	1.08	2.68	1.35
	S3	Oblique battlement-shaped reinforcement	1894	2127	1.12	4.48	2.26
	S4	Tensile strip	1894	2163	1.14	2.90	1.46
Group II	S5	None	2314	2630	1.14	1.76	1.00
	S6	Battlement-shaped reinforcement	2314	2567	1.11	2.57	1.46
	S7	Welded circular stirrup	2314	2706	1.17	2.73	1.55
	S8	Oblique battlement-shaped reinforcement	2314	2746	1.19	3.12	1.77
	S9	Tensile strip	2314	2726	1.18	2.59	1.47
	S10	Tensile strip	2314	2538	1.10	2.76	1.57